Computational methods for the robust optimization of the design of a dynamic aerospace system in the presence of aleatory and epistemic uncertainties

Emerald International Journal of Numerical Methods for Heat and Fluid Flow

Efficient simulations of detailed combustion fields via the lattice Boltzmann method

Journal:	*International Journal of Numerical Methods for Heat and Fluid Flow*
Manuscript ID:	Draft
Manuscript Type:	Research Article
Keywords:	Combustion, lattice Boltzmann method, slow invariant manifold

Efficient simulations of detailed combustion fields via the lattice Boltzmann method

1. Introduction and motivation

Accurate modeling of reactive flows requires the solution of a large number of conservation equations as dictated by detailed reaction mechanism. In addition to the sometimes prohibitively large number of variables introduced, the numerical solution of the governing equations has to face the stiffness due to the fast time scales of the kinetic terms (processes occurring on a wide range of scales ranging from seconds down to nanoseconds). In fact, chemistry acts on top of transport phenomena, whose time scales are typically of the order of millisecond down to microsecond. Those issues make computations of flames, where detailed chemistry is to be accounted, in two- and three-dimensional flows extremely time consuming, and have particularly negative impact on the lattice Boltzmann method (LBM), whose number of fields (distribution functions or populations) is significantly larger than the number of fields in conventional methods (density, momenta, temperature, species mass fractions) by a factor ranging from tens to hundreds for 2D and 3D simulations. Moreover, stiffness drastically affects the implementation of explicit numerical solvers (such as the LBM), where reducing the time step becomes compulsory in order to both avoid numerical instabilities and keep a satisfactory accuracy. As a matter of fact, the smallest time scale need to be resolved (with a dramatic increase of the computational time) even if we are only interested in the slow dynamics of the system. Finally, the larger the number of elementary reactions in a detailed combustion mechanism, the more intense the computational effort to evaluate the reaction rates, which typically involves the computation of demanding functions (e.g. exponential functions).

For these reasons, techniques capable to reduce the computational time and the memory demand are particularly desirable in the contest of the lattice Boltzmann method when simulating reactive flows. In this respect, some reduction might be achieved without a big effort , e.g., by eliminating unimportant reaction steps (or species) from the detailed combustion mechanism. Several tools have been devised to that aim, such as the sensitivity analysis [1], the comparative analysis of entropy production [2, 3], and the reaction path analysis [4]. Nevertheless, the above methodologies are never fully automated, and they often produce results with unsatisfactory accuracy. In the following, we make use of a model reduction technique, the *Method of Invariant Grid* [10] (MIG), based on the notions of time-scale separation and low dimensional manifolds, which present the advantage of an automated implementation (see, e.g., [19]) and it is expected to recover the asymptotic behavior of the detailed system, with remarkable accuracy [9, 17]. In fact, we are often interested in the system behavior on the scale of fluid mechanics (slow dynamics), thus some chemical phenomena (fast dynamics) can be considered self-equilibrated. The general idea behind MIG stems from the geometric picture of relaxation of solution trajectories in the phase-space, and is briefly described below. Dynamics of complex reactive system is often characterized by a short initial transient during which the fast processes evolve and equilibrate, such that the solution trajectory approaches low-dimensional manifolds in the concentration space, known as the *slow invariant manifolds* (SIM). The remaining dynamics lasts much longer and evolves along the SIM towards the steady state (see also the section 4.2 and Fig. 2 below). Decoupling the fast equilibrated processes from the slower dynamics does indeed bring a reduction of degrees of freedom into the problem, and can be implemented in a systematic manner by devising effective techniques for constructing SIM in the solution space of the detailed system.

The notion of low dimensional manifold of slow motions has proved fruitful in model reduction, and it has been widely investigated in chemical kinetics for analyzing and simplifying complex reaction mechanisms. Besides the already mentioned MIG by Gorban and Karlin, the most popular methods based on the above concept are, among others: the Computational Singular Perturbation Method (CSP) by Lam and Goussis [5], the *Intrinsic Low Dimensional Manifold* (ILDM) by Maas and Pope [6], the *Invariant Constrained Equilibrium Edge Preimage Curve Method* (ICE-PIC) by Ren, Pope et al. [7], and the *Method of Minimal Entropy Production Trajectories* (MEPT) by Lebiedz [8].

This work is organized in sections as follows. In section 2, the kinetic equations describing reactive mixtures are reviewed, and the case of a batch reactor under fixed enthalpy and pressure discussed in more detail. The lattice Boltzmann model for reactive flow simulation, adopted in the following, and the hypotheses behind it are reviewed in section 3. Some basics about the MIG technique are discussed in section 4. In particular, the notions of quasi equilibrium manifold, film equation and thermodynamic projector are reviewed in sections 4.1 and 4.2, while their application to a bath reactor is reported in section 4.3. The coupling between the MIG and the lattice Boltzmann model is studied in section 5, and applied to a two-dimensional laminar flame in sections 5.2 and 5.3. In section 6, the limits of validity of the presented methodology are discussed, and possible extensions oulined. In section 7 conclusions are drawn.

2. Gas mixtures in a batch reactor

Below, we focus on mixtures of ideal gases, where n chemical species $x_1, ..., x_n$ are involved in a complex reaction consisting of r reversible elementary steps as follows:

$$\nu'_{s1}x_1 + \ldots + \nu'_{sn}x_n \rightleftarrows \nu''_{s1}x_1 + \ldots + \nu''_{sn}x_n, \quad s = 1, \ldots, r, \tag{1}$$

with ν'_{si} and ν''_{si} the stoichiometric coefficient of species i in the reaction step s in the forward and reverse direction, respectively. The reaction rate due to step s takes the expression:

$$\Omega_s = k_s^f \prod_{j=1}^{n} [X_j]^{\nu'_{js}} - k_s^r \prod_{j=1}^{n} [X_j]^{\nu''_{js}}, \quad s = 1, \ldots, r, \tag{2}$$

where $[X_j]$ denotes the molar concentration of species j. The rate of production (or consumption) of species i in reaction s reads:

$$\dot{\omega}_{is} = \left(\nu''_{is} - \nu'_{is}\right) \Omega_s. \tag{3}$$

Both the forward and reverse reaction rate constants k_s^f and k_s^r are typically expressed using the popular semi-empirical modified Arrhenius formula:

$$k_s\left(T\right) = A_s T^{\beta_s} \exp\left(-E_{as}/\mathcal{R}T\right), \tag{4}$$

where A_s is a pre-exponential factor, β_s the temperature exponent, E_s the activation energy of step s and $\mathcal{R}$ the universal gas constant. The total production (or consumption) rate of species i reads:

$$\dot{\omega}_i = \sum_{s=1}^{r} \dot{\omega}_{is}, \tag{5}$$

with the forward and reverse reaction rate constants related by the equilibrium constant $K_{c,s} = k_s^f \Big/ k_s^r$, which is obtained imposing the *principle of detail balance* at the steady state:

$$k_s^f \prod_{j=1}^{n} [X_j]^{\nu'_{js}} = k_s^r \prod_{j=1}^{n} [X_j]^{\nu''_{js}}, \quad s = 1, \ldots, r. \tag{6}$$

In batch reactors, the gas mixture is a closed system with no mass flux through the boundary, and the state $\boldsymbol{\psi} = (Y_1, \ldots, Y_n)$ evolves in time according to:

$$\vec{f} = \left(\frac{dY_1}{dt}, \ldots, \frac{dY_n}{dt} \right) = \left(\frac{\dot{\omega}_1 W_1}{\bar{\rho}}, \ldots, \frac{\dot{\omega}_n W_n}{\bar{\rho}} \right), \tag{7}$$

where Y_i and W_i are the mass fraction and the molecular weight of species i respectively, while $\bar{\rho}$ represents the mixture mean density. In order to close the kinetic equation system (7), an additional condition for the temperature dynamics is required. In the following, we refer to closed isoenthalpic isobaric systems where the equation for temperature stipulates the constance of the mixture averaged enthalpy $\bar{h}$:

$$\bar{h} = \sum_{i=1}^{n} h_i(T)\, Y_i = const, \tag{8}$$

where h_i denotes the enthalpy of species i, whose temperature dependence is accounted using a polynomial fit

$$h_i(T) = R \left(a_{1i} T + \frac{a_{2i}}{2} T^2 + \frac{a_{3i}}{3} T^3 + \frac{a_{4i}}{4} T^4 + \frac{a_{5i}}{5} T^5 + a_{6i} \right), \tag{9}$$

expressed in terms of the NASA coefficients a_{ij}, tabulated for each species i, with $j = 1, ..., 7$. More specifically, the temperature dynamics obeys the following equation:

$$\bar{c}_p \frac{dT}{dt} = -\frac{1}{\bar{\rho}} \sum_{i=1}^{n} h_i \dot{\omega}_i W_i. \tag{10}$$

Finally, in a closed reactor, the atom mole numbers N_k of each element k is conserved:

$$\boldsymbol{D}\boldsymbol{\psi}^T = (N_1, \ldots, N_d)^T, \quad \frac{dN_k}{dt} = 0, \quad \boldsymbol{D}(k,i) = \frac{\mu_{ik}}{W_i}. \tag{11}$$

Here, μ_{ik} is the number of atoms of the kth element in species i, and $\boldsymbol{D}$ is a $(d \times n)$ matrix, where d is the number of elements involved the reaction. In other words, the vector field $\vec{f}$ in (7) remains always orthogonal (in the Euclidean sense) to the raws of $\boldsymbol{D}$.

3. Model for reactive flow simulations

In the present work, for the sake of simplicity, we apply the following assumptions to the governing equations for reactive flows in the low Mach number regime:

- The flow field is assumed incompressible and it is not affected by the chemical reaction.
- The transport properties are constant.
- The Fick's law applies to diffusion.
- Viscous energy dissipation and radiative heat transfer can be neglected.

It's worth noticing that we make use of the above simplifications, since they are not essential to the issues of model reduction for reactive flows simulations, which is our major concern here. In fact, the suggested methodology can be applied also when all the above hypothesis are relaxed. In such a framework, the velocity field u_i and pressure p can be described by solving the mass and momentum

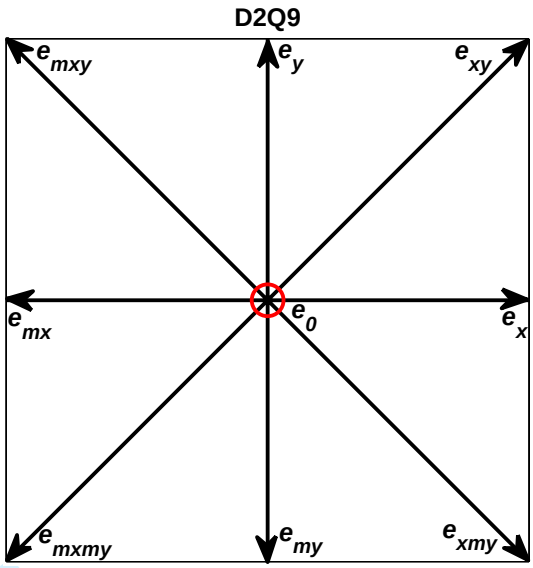

FIGURE 1. 2-dimensional 9-velocity stencil: D2Q9

conservation equations as dictated by the incompressible Navier-Stokes formulation (in the absence of body forces):

$$\begin{aligned} &\partial_j u_j = 0, \\ &\partial_t u_i + u_j \partial_j u_i = -\tfrac{1}{\bar{\rho}} \partial_i p + \partial_j \left(\nu \partial_j u_i \right), \end{aligned} \tag{12}$$

where ∂_t, ∂_j, ν and $\bar{\rho}$ denote partial derivatives with respect to time, partial derivatives with respect to the jth spacial direction, the kinematic viscosity and the mixture density respectively, while Einstein summation convention is assumed for the repeated indexes. Moreover, the governing equations of the mixture-averaged enthalpy $\bar{h}$ and the mass fraction Y_i of the ith chemical species has to be taken into account as follows:

$$\partial_t \bar{h} + u_j \partial_j \bar{h} = \partial_j \left(\kappa \partial_j \bar{h} \right) + \sum_{i=1}^{n} \frac{\dot{\omega}_i W_i}{\bar{\rho}} h_i, \tag{13}$$

$$\bar{\rho} \left(\partial_t Y_i + u_j \partial_j Y_i \right) = \partial_j \left(\bar{\rho} D_i \partial_j Y_i \right) + \dot{\omega}_i W_i, \tag{14}$$

where κ and D_i are the thermal diffusivity and the diffusion coefficient of species i, respectively.

3.1. **Lattice Boltzmann method for combustion.** Here, we consider the simple lattice Boltzmann formulation suitable for combustion field computations suggested in [21], whereas more elaborate LB models for mixtures [22] and compressible flows [23] shall be investigated in the near future, too. It has been proven that model in [21] is able to describe reactive flows consistently with the continuum approach where the equations (12), (13) and (14) are used.

The lattice Boltzmann method is a relatively novel approach to numerical flow simulations, and it can be regarded as a special discretization of the Boltzmann equation which is known to be the governing equation of gas dynamics [25]. This method consists of discrete and explicit kinetic equations expressed in terms of a small set of particles distribution functions (populations for short). Those kinetic equations are designed in such a way that the the continuum description (Navier-Stokes equations) is recovered in the hydrodynamic limit, where the Knudsen number is small. Each population moves on a regular lattice at a different velocity: in Fig. 1 we show a popular scheme for two-dimensional simulations, where nine populations are represented by their own peculiar velocity $\boldsymbol{e}_\alpha$.

In the following, the flow field is treated as a single-component medium that can be described, in terms of pressure distribution functions p_α, by the following equation at an arbitrary lattice node $\boldsymbol{x}$ [25]:

$$p_\alpha\left(\boldsymbol{x}+\boldsymbol{e}_\alpha, t+\delta t\right)=p_\alpha\left(\boldsymbol{x}, t\right)-\frac{1}{\tau_F}\left[p_\alpha\left(\boldsymbol{x}, t\right)-p_\alpha^{eq}\left(p, \boldsymbol{u}\right)\right], \tag{15}$$

where the equilibrium populations p_α^{eq} read:

$$p_\alpha^{eq}=w_\alpha p\left[1+3\left(\boldsymbol{e}_\alpha \boldsymbol{u}^T\right)+\frac{9}{2}\left(\boldsymbol{e}_\alpha \boldsymbol{u}^T\right)^2-\frac{3}{2}\boldsymbol{u}^2\right]. \tag{16}$$

The pressure p and the fluid velocity $\boldsymbol{u}$ are given by:

$$p=\sum_\alpha p_\alpha, \quad \boldsymbol{u}=\frac{1}{p_0}\sum_\alpha \boldsymbol{e}_\alpha p_\alpha, \tag{17}$$

where the reference pressure $p_0=\rho_0/3$, with ρ_0 denoting the reference density of the LB model. Let δt be the time step, the relaxation parameter τ_F can be linked to the kinematic viscosity ν, e.g., by performing an asymptotic analysis of the lattice Boltzmann equation (see, e.g., [27, 28])

$$\nu=\frac{2\tau_F-1}{6}\delta t. \tag{18}$$

In general, the discrete velocities can be regarded as the nodes of a Gauss-Hermite quadrature applied to the Maxwell-Boltzmann distribution function, and each of them is characterized by a proper weight w_α (see also [25, 26]). According to [21], the flow field is not affected by the chemical reaction, transport coefficients are constant and Fick's law applies to the diffusion. Let $\bar{h}_0$ be a reference enthalpy, the evolution equations for enthalpy and concentration of species i are written as

$$\tilde{h}_\alpha\left(\boldsymbol{x}+\boldsymbol{e}_\alpha, t+\delta t\right)-\tilde{h}_\alpha\left(\boldsymbol{x}, t\right)=-\frac{1}{\tau_h}\left[\tilde{h}_\alpha\left(\boldsymbol{x}, t\right)-\tilde{h}_\alpha^{eq}\left(\tilde{h}, \boldsymbol{u}\right)\right]+w_\alpha Q_h, \tag{19}$$

$$Y_{i\alpha}\left(\boldsymbol{x}+\boldsymbol{e}_\alpha, t+\delta t\right)-Y_{i\alpha}\left(\boldsymbol{x}, t\right)=-\frac{1}{\tau_{Y_i}}\left[Y_{i\alpha}\left(\boldsymbol{x}, t\right)-Y_{i\alpha}^{eq}\left(Y_i, \boldsymbol{u}\right)\right]+w_\alpha Q_{Y_i}, \tag{20}$$

where

$$\tilde{h}=\bar{h}/\bar{h}_0=\sum_\alpha \tilde{h}_\alpha, \quad Y_i=\sum_\alpha Y_{i\alpha}, \tag{21}$$

and the equilibrium populations $\tilde{h}_\alpha^{eq}$, $Y_{i\alpha}^{eq}$ are expressed as in (16) after replacing p with $\tilde{h}$ and Y_i, respectively. Assume t_0 is a factor for converting physical time into LB time units: $(t)_{LB}=(t)_{phys}\big/t_0$, the source terms take the explicit form

$$Q_h=\frac{1}{h_0}\left(\sum_{i=1}^{9}\frac{\dot{\omega}_i W_i}{\bar{\rho}}h_i\right)t_0\delta t,\ Q_{Y_i}=\frac{\dot{\omega}_i W_i}{\bar{\rho}}t_0\delta t, \tag{22}$$

where $\bar{\rho}$ is the mixture-averaged density, while $\dot{\omega}_i$, W_i, h_i denote the rate of change, molecular weight and enthalpy of species i, respectively. Similarly to the kinematic viscosity, the thermal diffusivity κ and diffusion coefficient D_i of species i are related to the relaxation parameters as follows:

$$\kappa=\frac{2\tau_h-1}{6}\delta t, \quad D_i=\frac{2\tau_{Y_i}-1}{6}\delta t. \tag{23}$$

4. Model reduction technique

In our study, the reduced model is obtained using the *Method of Invariant Grid* (MIG). The detailed mechanism of Li et al [11] (9 species, 21 elementary reactions) for hydrogen combustion is considered, and our goal is to search for a reduced description with only a few degrees of freedom. In particular,

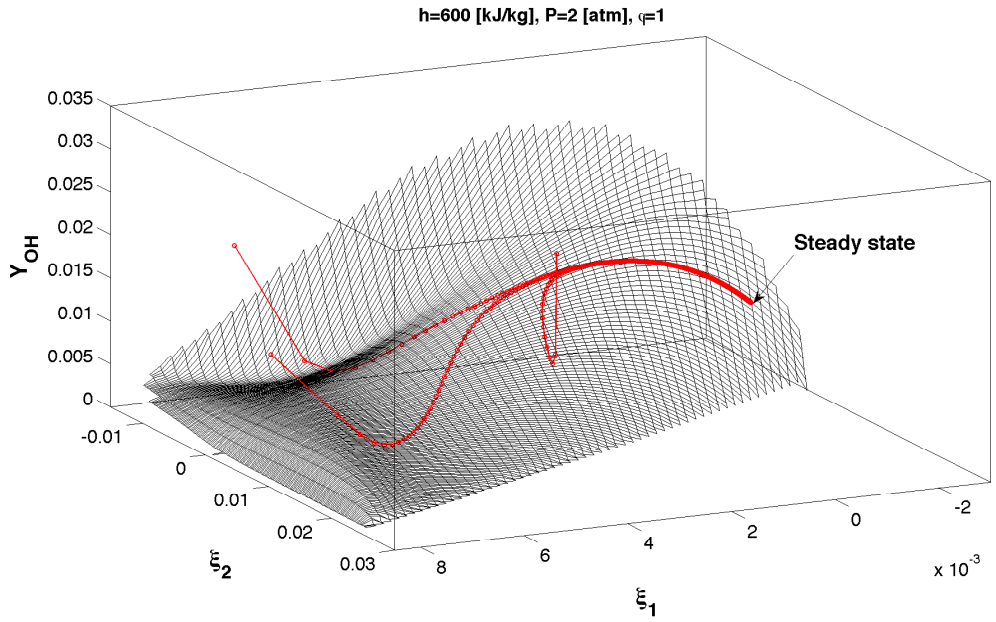

FIGURE 2. Batch reactor under constant enthalpy and pressure at stoichiometric proportions. Example of a 2D invariant grid (black continuous lines). Samples of solutions trajectories (circles) relaxing towards the grid are reported.

here we are interested in a reduced description, where the combustion mechanism is governed by two chemical coordinates. Below, a general overview of MIG method is given, while more details can be found in the literature [9, 10, 15, 16, 17].

4.1. **MIG initialization.** For our purposes, the MIG technique can be initially applied to a spatially homogeneous reactor under constant mixture-averaged enthalpy and pressure at a fixed equivalence ratio ϕ. To this end, we first construct a two-dimensional *quasi-equilibrium manifold* (QEM) for a stoichiometric H_2-air mixture under fixed pressure p and enthalpy $\bar{h}$. In general, a $q-$ dimensional QEM is obtained solving the following minimization problem:

$$\text{(24)} \qquad \begin{cases} G \to \min \\ \sum_i m_j^i Y_i = \xi^j, \quad j = 1, \dots, q, \end{cases}$$

where G is a thermodynamic Lyapunov function with respect to the kinetic equations (7). It is well known from thermodynamics that, in a closed reactive system under fixed enthalpy and pressure, the latter function is given by the mixture-averaged entropy. Moreover, the vector set $\{\boldsymbol{m}_j = (m_j^1, ..., m_j^9)\}$ is adopted in order to re-parameterize the primitive variables Y_i (mass fraction) in terms of new lumped quantities ξ^j, whose dynamics is expected to be slower than Y_i. Quasi equilibrium manifolds attempt a fast-slow motion decomposition of the kinetic system dynamics, where the slow movements are assumed to occur (throughout the entire composition space) in the subspace spanned by the vectors $\boldsymbol{m}_j$, while fast motions occur in its orthogonal complement. The notion of QEM can provide with an approximated reduced description in chemical kinetics at a reasonable computational cost, hence it has been widely exploited for that purpose (see, e.g., [13, 12, 15]). Several suggestions for defining slow lumped variables in chemical kinetics are known from the literature. It is worth to mention here, the parameterization utilized in the *Rate Controlled Constrained Equilibrium* (RCCE) method [14] where a physical meaning is directly attached to the slow parameters ξ. For instance in the case of hydrogen

combustion, the following quantities

$$\xi^1 = \sum_i \frac{Y_i}{W_i}, \quad \xi^2 = \frac{Y_O}{W_O} + \frac{Y_{OH}}{W_{OH}} + \frac{Y_{H_2O}}{W_{H_2O}}, \quad \xi^3 = \frac{Y_H}{W_H} + 2\frac{Y_O}{W_O} + \frac{Y_{OH}}{W_{OH}}, \tag{25}$$

related to the total number of moles, the number of moles of free oxygen and the active valence respectively, may be adopted for constructing up to three-dimensional quasi equilibrium manifolds (see also [12]). Moreover, a more systematic parameterization of a quasi equilibrium manifold has been introduced recently [16], where the vectors $\boldsymbol{m}_j$ are defined on the basis of the left eigenvectors of the Jacobian matrix

$$\boldsymbol{J} = \begin{bmatrix} \frac{\partial f_1}{\partial Y_1} & \cdots & \frac{\partial f_1}{\partial Y_n} \\ \vdots & \ddots & \vdots \\ \frac{\partial f_n}{\partial Y_1} & \cdots & \frac{\partial f_n}{\partial Y_n} \end{bmatrix}, \tag{26}$$

computed a the steady state: *spectral quasi equilibrium manifold*. Here, f_i is the ith component of the vector field (7). Notice that, in the following we always deal with a discrete representation of a manifod (*grid*), namely sets of states (points in the concentration space) and connections between them that allow us to define the grid tangent space at each node.

An approximated solution to (24), called *quasi equilibrium grid* (QEG), can be computed making use of the algorithm introduced in [15] and briefly reviewed below. According to the latter algorithm, an initial grid is constructed starting from a known state (*seed*) of the quasi equilibrium manifold (typically the steady state) upon linearization of the problem (24). Therefore, extension of a grid along the $k-$th parameter ξ^k is accomplished by solving the linear system:

$$\begin{aligned} &\sum_{i=1}^{z} \left(\boldsymbol{t}_j \boldsymbol{H} \boldsymbol{\rho}_i^T\right) \varphi_i = -\boldsymbol{t}_j \boldsymbol{\nabla} G^T, \quad j = 1, \ldots, z-q \\ &\sum_{i=1}^{z} \left(\boldsymbol{m}_1 \boldsymbol{\rho}_i^T\right) \varphi_i = 0, \\ &\vdots \\ &\sum_{i=1}^{z} \left(\boldsymbol{m}_k \boldsymbol{\rho}_i^T\right) \varphi_i = \varepsilon_k, \\ &\vdots \\ &\sum_{i=1}^{z} \left(\boldsymbol{m}_q \boldsymbol{\rho}_i^T\right) \varphi_i = 0, \end{aligned} \tag{27}$$

with respect to the unknowns φ_i, where $\boldsymbol{\nabla} G$ and $\boldsymbol{H}$ signify the gradient and the second derivative matrix of G, respectively, computed at the seed, under constant mixture enthalpy $\bar{h}$ and pressure p. Let $\boldsymbol{E}$ be a matrix obtained from $\boldsymbol{D}$ by adding the parameterization vectors $\boldsymbol{m}_j$ as additional rows, the two vector bases $\{\boldsymbol{\rho}_1, \ldots, \boldsymbol{\rho}_z\}$ and $\{\boldsymbol{t}_1, \ldots, \boldsymbol{t}_{z-q}\}$ span the null space of $\boldsymbol{D}$ and $\boldsymbol{E}$, respectively. Let $\boldsymbol{c}^0 = \left(c_1^0, \ldots, c_n^0\right)$ be the seed, the new QE-grid state $\boldsymbol{c}^1$, in a neighborhood of $\boldsymbol{c}^0$, has the following coordinates:

$$\begin{aligned} \boldsymbol{c}^1 &= \left(c_1^0 + dc_1^0, \ldots, c_n^0 + dc_n^0\right), \\ \left(dc_1^0, \ldots, dc_n^0\right) &= \sum_{i=1}^{z} \varphi_i \boldsymbol{\rho}_i. \end{aligned}$$

When dealing with isobaric isenthalpic systems, G is related to the mixture averaged entropy $\bar{s}$ which, for ideal gas mixtures, takes the following explicit form:

$$G_{p,\bar{h}} = -\bar{s} = -\frac{1}{\bar{W}} \sum_{i=1}^{n} \left[s_i(T) - \mathcal{R} \ln\left(X_i\right) - \mathcal{R} \ln\left(\frac{p}{p_{ref}}\right) \right] X_i, \tag{28}$$

where $\bar{W}$, $\mathcal{R}$, X_i, p and p_{ref} denote the mean molecular weight, the universal gas constant, the mole fraction of species i, the total pressure and a reference pressure, respectively. The specific entropy s_i is assumed to have the following dependence on the temperature T:

$$s_i(T) = \mathcal{R}\left(a_{i1}\ln T + a_{i2}T + \frac{a_{i3}}{2}T^2 + \frac{a_{i4}}{3}T^3 + \frac{a_{i5}}{4}T^4 + a_{i7}\right) \tag{29}$$

where, for each chemical species i, a_{ij} are given by the NASA coefficients.

In the following, in order to save notation, it proves convenient to define both the following *entropic scalar product* between two arbitrary vectors $\boldsymbol{x}$ and $\boldsymbol{y}$:

$$\langle \boldsymbol{x}, \boldsymbol{y} \rangle = \boldsymbol{x}\boldsymbol{H}\boldsymbol{y}^T, \tag{30}$$

and the functional

$$DG(x) = \boldsymbol{\nabla} G \boldsymbol{x}^T \tag{31}$$

where the superscript ^{T} signifies transposition.

Finally, notice that computing first and second derivative of G is not straightforward, since (28) explicitly depends on the mixture temperature T, which is in turn implicit function of the enthalpy $\bar{h}$ as dictated by the non-linear relation (9). However, to this end, both approximate, e.g. *finite differencing* (FD), and exact approaches, e.g. *automatic differentiation* (AD), can be adopted. According to FD, the exact fist derivative is approximated by the following ratio:

$$\left.\frac{\partial G}{\partial Y_i}\right|_{p,\bar{h}} \simeq \frac{G(T', \ldots, Y_i + \varepsilon, \ldots) - G(T', \ldots, Y_i, \ldots)}{\varepsilon}, \tag{32}$$

where ε is a small parameter, while the temperature T' satisfies the following equation:

$$\bar{h}\left(T', \ldots, Y_i + \varepsilon, \ldots\right) = \bar{h}\left(T', \ldots, Y_i, \ldots\right). \tag{33}$$

Typically, in order to achieve the best accuracy and minimize the round-off error, ε is chosen of the order of the square root of the machine precision. Moreover, forward (or backward) finite difference schemes are preferred for first derivatives, and central schemes are adopted for second derivatives. On the other hand, AD enables to differentiate (in principle up to any order) the subroutine itself that computes the function (28), by systematically applying chain rule to the entire sequence of elementary assignments of the code. Although AD can be significantly slower than FD (up to an order of magnitude), it provides with exact values of the derivatives. Alternatively, the explicit and exact formulas reported in [19] can be adopted.

4.2. **MIG refinements.** It is worth stressing that the choice of the vector set $\boldsymbol{m}_j$ has a significant influence on the accuracy of the corresponding QEM in describing the slow invariant manifold (see [16]). Nevertheless, the above construction only represents the first step of the MIG technique, given that a QE-grid $\mathcal{G}$ has to be anyway refined as described below in this section. The refined grid (*invariant grid*) is an accurate discrete approximation of the slow invariant manifold, hence it does not depend on the chosen parameterization.

Let $\mathcal{G}$ be given by a unique mapping $\boldsymbol{c} = F\left(\xi^1, \ldots, \xi^q\right)$ defined in a discrete subset of the parameter space into the concentration space. We also assume that there is a reconstruction procedure (e.g. polynomial interpolation), such that derivatives $\partial F / \xi^i$ can be computed and the local tangent space to $\mathcal{G}$ defined.

According to MIG, the invariant grid of the kinetic system can be computed by relaxation of $\mathcal{G}$ under the following film equation of dynamics [9]

$$\frac{d\mathcal{G}}{dt} = \vec{f} - \boldsymbol{P}\vec{f}, \tag{34}$$

where $\vec{f}$ and $\boldsymbol{P}$ denote the vector of motion in the phase space and a projector operator onto the grid tangent space, respectively. In general, the operator $\boldsymbol{P}$ can be any matrix which satisfies the condition $\boldsymbol{P}^2 = \boldsymbol{P}$, such that the vector $\boldsymbol{P}\vec{f}$ belongs to the tangent space. Here, however, we adopt the *thermodynamic projector* [20], which enables to identify the fast motions toward the slow manifolds.

The thermodynamic projector is based on the following idea: If a given manifold indeed represents the manifold of slow motions, then the Lyapunov function G has been increasing during the fast process of relaxation towards this manifold. Therefore, the points of the manifold appear as the minimum points of the Lypunov function on the manifolds of fast motion. The latter can be approximated accurately in a small vicinity of the slow manifold using the Lyapunov function gradient at the points of SIM. The thermodynamic projector $\boldsymbol{P}$ in fact formalizes this intuitive picture as reported below. Importantly, $\boldsymbol{P}$ is updated on each iterations when seeking the SIM from the film equation.

Let the derivatives $\partial F/\partial \xi^i$ define the tangent space $T_{\boldsymbol{c}}$, at each grid point $\boldsymbol{c}$:

$$T_{\boldsymbol{c}} = Lin\left\{\partial F/\partial \xi^i\right\}, \quad i = 1, ..., q. \tag{35}$$

The subspace $T_{\boldsymbol{c},0} = (T_{\boldsymbol{c}} \cap \ker DG)$ defines, if $T_{\boldsymbol{c}} \neq T_{\boldsymbol{c},0}$, the tangent vector $\boldsymbol{e} \in T_{\boldsymbol{c}}$, through the following conditions:

$$DG(\boldsymbol{e}) = 1, \quad \langle \boldsymbol{e}, \boldsymbol{x} \rangle = 0, \quad \forall \boldsymbol{x} \in T_{\boldsymbol{c},0}, \tag{36}$$

so that, the thermodynamic projection of an arbitrary vector $\boldsymbol{x}$ has the form:

$$\boldsymbol{P}\boldsymbol{x} = DG(x)\,\boldsymbol{e} + \sum_{i=1}^{q-1} \langle \boldsymbol{k}_i, \boldsymbol{x} \rangle \boldsymbol{k}_i. \tag{37}$$

The basis $\{\boldsymbol{k}_1, \ldots, \boldsymbol{k}_{q-1}\}$ (orthonormal with respect to the entropic scalar product (30)) spans the subspace $T_{\boldsymbol{c},0}$. In the case $T_{\boldsymbol{c}} \equiv T_{\boldsymbol{c},0}$, the projector (37) becomes:

$$\boldsymbol{P}\boldsymbol{x} = \sum_{i=1}^{q} \langle \boldsymbol{k}_i, \boldsymbol{x} \rangle \boldsymbol{k}_i. \tag{38}$$

Remark. Here, it is worth stressing the relevant feature of the latter projector. Let us consider a q-dimensional SIM in a n-dimensional phase space. The above construction is based on the idea that the thermodynamic considerations (minimization of the thermodynamic Lyapunov function) are solely required to construct fast manifolds in the vicinity of SIM. On the other hand, if it is possible to describe the fast subspace in different terms (for example, as a result of a different algorithm for construction of SIM), both representations of fast motions should be consistent. Let a vector $\boldsymbol{a}_{r_i}(\boldsymbol{c})$ be a generic vector of the fast subspace. Then

$$\boldsymbol{a}_{r_i}(\boldsymbol{c}) \in \ker \boldsymbol{P}, \qquad \forall i = 1, ..., n - q, \tag{39}$$

where $\ker \boldsymbol{P}$ is the null space of (37) evaluated at $\boldsymbol{c}$. In other words, the thermodynamic projection of fast directions, in a neighborhood of the SIM vanishes.

Finally, as an example, a two-dimensional quasi equilibrium grid of a reactive H_2-air mixture with $\bar{h} = 600kJ/kg$, $p = 2bar$ and $\phi = 1$ is constructed as illustrated in the above section 4.1, making use of the spectral quasi equilibrium parameterization. The refined grid is shown in Fig. 2, where typical solution trajectories attracted to the grid and relaxing towards the steady state are also reported.

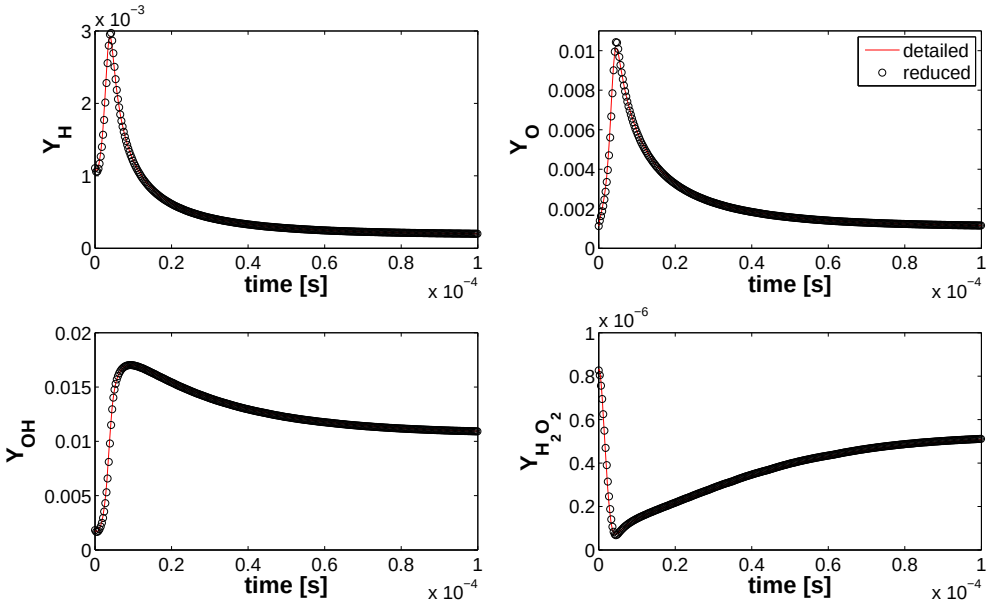

FIGURE 3. Batch reactor under constant enthalpy and pressure at stoichiometric proportions. Specie mass fraction dynamics, as dictated by the detailed model (continuous lines), is compared to the corresponding reduced model solution, where the initial condition belongs to a 2D invariant grid.

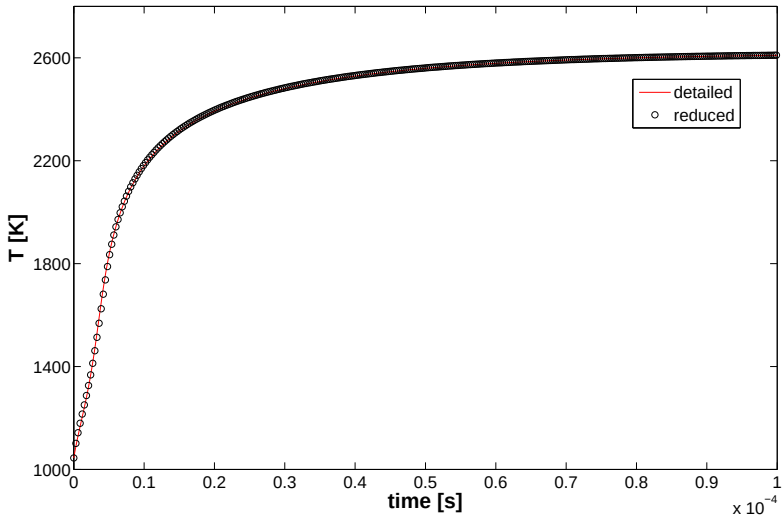

FIGURE 4. Batch reactor under constant enthalpy and pressure at stoichiometric proportions. Temperature dynamics, as dictated by the detailed model (continuous lines), is compared to the corresponding reduced model solution, where the initial condition belongs to a 2D invariant grid.

4.3. **Integration of the reduced system.** Once a $q-$dimensional invariant grid is constructed (typically with $q \ll n$), the set of kinetic equations (7) (problem with $(n-d)$ degrees of freedom) admits a reduced description with q degrees of freedom. In fact, the system dynamics along invariant grids

$$\left(\frac{dY_1}{dt}, \ldots, \frac{dY_n}{dt}\right)^T = \boldsymbol{P}\vec{f}, \tag{40}$$

can be recast in a smaller set of differential equations, by recalling the definition of the parameters ξ^i:

$$\left(\frac{d\xi^1}{dt}, ..., \frac{d\xi^q}{dt}\right) = \left(\boldsymbol{m}_1 \boldsymbol{P}\vec{f}, \ldots, \boldsymbol{m}_q \boldsymbol{P}\vec{f}\right). \tag{41}$$

Notice that, the projector $\boldsymbol{P}$ of the reduced systems (40) and (41) must be constructed as prescribed in section 4.2. Indeed, in this case, the fast directions belong to the null space of the thermodynamic projector, and the right-hand side of (40) and (41) is characterized by a reduced stiffness with respect to the original system (7). The right-hand side of (41) can be tabulated along with the node coordinates and the parameters ξ^j, before solving the reduced system. However, a reconstruction procedure, such as a multi-variate interpolation, is typically adopted in order to evaluate the rates (41) at an arbitrary point of the phase-space.

Using the two-dimensional invariant grid depicted in Fig. 2, we report a comparison between the solution of the detailed kinetic model (7) an the reduced one (41), starting from an arbitrary initial condition of the grid (see Fig. 3 and 4). Excellent agreement between the two descriptions can be observed, whereas the time step used in the numerical solver (explicit fourth order Runge-Kutta) of the reduced model can be chosen an order of magnitude larger than the one for the detailed one, due to the reduced stiffness of (41).

5. 2D PREMIX LAMINAR FLAME

In this section, we illustrate the coupling methodology between a reduced model obtained from the MIG procedure, and the lattice Boltzmann model for reactive flows reviewed in section (3). For simplicity, in the following, we use the assumption of equal diffusivity D for all species and Lewis number $Le = \kappa/D = 1$. In this case, the mixture enthalpy $\bar{h}$ and the element fractions remain constant throughout the domain, and the reduced dynamics takes place along a single invariant grid. Notice however that, the latter assumption is not restricting and a generalization is obtained by extending the invariant grid with enthalpy and element fractions as additional degrees of freedom (see also the section 6 below). Moreover, in low-Mach combustion, the pressure p can be considered constant for most cases. Under the latter assumptions, the equations (20) can be written in terms of the slow manifold parameters ξ^1, ξ^2 as follows:

$$\xi_\alpha^j\left(\boldsymbol{x} + \boldsymbol{e}_\alpha, t + \delta t\right) - \xi_\alpha^j\left(\boldsymbol{x}, t\right) = -\frac{1}{\tau_\xi}\left[\xi_\alpha^j(\boldsymbol{x}, t) - \xi_\alpha^{jeq}\left(\xi^j, \boldsymbol{u}\right)\right] + w_\alpha Q_{\xi^j}, \tag{42}$$

where, the equilibrium populations for the reduced variables ξ^j read

$$\xi_\alpha^{jeq} = w_\alpha \xi^j \left[1 + 3\left(\boldsymbol{e}_\alpha \boldsymbol{u}^T\right) + \frac{9}{2}\left(\boldsymbol{e}_\alpha \boldsymbol{u}^T\right)^2 - \frac{3}{2}\boldsymbol{u}^2\right], \tag{43}$$

and the source terms take the form:

$$Q_{\xi^j} = \sum_{i=1}^{9} m_j^i Q_{Y_i},\ \xi^j = \sum_{i=1}^{9} m_j^i Y_i. \tag{44}$$

5.1. **Example.** Here, we consider the two-dimensional laminar burner schematically represented in Fig. 5, where several vertical nozzles, ejecting a premixed mixture of hydrogen and air, are put side by side at a fixed distance. A fully premixed hydrogen/air mixture, initially at room temperature (300 K), is ignited by a spark which is simulated by placing a hot spot in a corner of the computational domain. A propagating flame front is thus generated in the flow, while the burned gas exits from the top side of the domain. Because of the geometric symmetry, and under the assumption of laminar flow, the

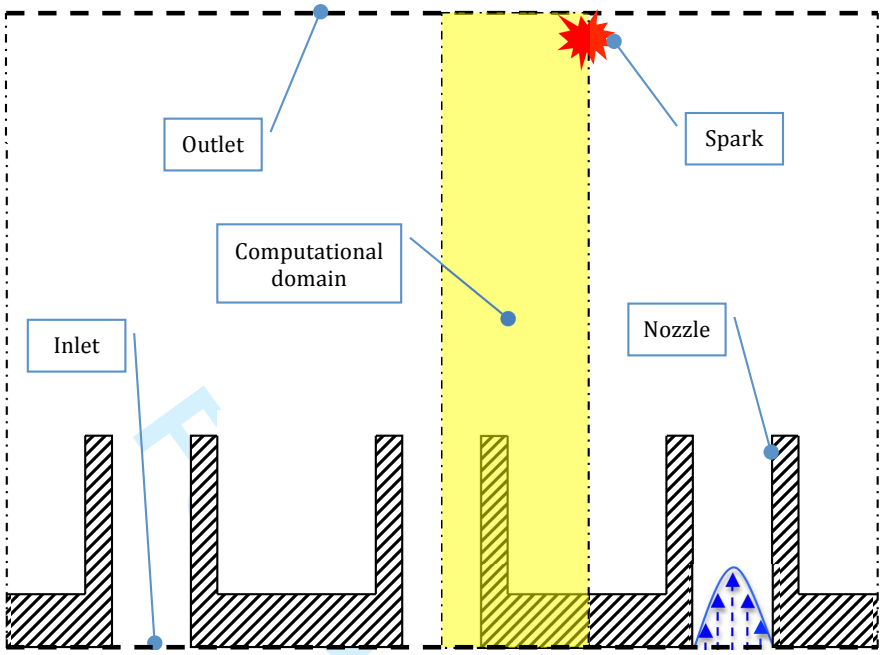

FIGURE 5. Sketch of a 2-dimensional burner. Due to the symmetric geometry, computations can be restricted to a rectangular domain.

computations can be restricted to a rectangular domain, whose left and right edges are both symmetry axis (see Fig. 5). In the present configuration, the burner slot is $0.4[mm]$ wide, the nozzle thickness and the domain height are assumed $0.1[mm]$ and $7.31[mm]$ respectively, while the distance between the centerlines of two contiguous nozzles is $2.84[mm]$. Note that, each single nozzle can be considered a two-dimensional representation of a *Bunsen burner*. The flame dynamics might be predicted by solving both the detailed model (19), (20) and the reduced one (42). In the following, we focus on the latter option, where the source terms Q_{ξ^j} are tabulated at each node of the invariant grid, and accessed through multi-variate linear interpolation.

Notice that, all the quantities in LB units are dimensionless, thus transport coefficients and chemical source terms need to be properly converted with the help of analogy. Let L_{phys} and u_{phys} be the height of the computational domain and the norm of flow velocity at the inlet along the symmetry axis in physical units, respectively: $[m]$ and $[m/s]$. Let L_{LB} and u_{LB} be the corresponding dimensionless quantities (LB units). It proves convenient to define the following conversion factors:

$$t_0 = \left(\frac{L_{phys}}{u_{phys}}\right) \Big/ \left(\frac{L_{LB}}{u_{LB}}\right), \quad L_0 = \frac{L_{phys}}{L_{LB}}, \tag{45}$$

such that physical time expressed in $[s]$ and length in $[m]$ can be converted into LB units dividing by t_0 and L_0, respectively. For instance, the diffusion coefficient D_i ($[m^2/s]$) and the source term $\frac{\dot{\omega}_i W_i}{\bar{\rho}}$ ($[s^{-1}]$) of species i become in LB units:

$$(D_i)_{LB} = D_i \frac{t_0}{L_0^2}, \quad \left(\frac{\dot{\omega}_i W_i}{\bar{\rho}}\right)_{LB} = \frac{\dot{\omega}_i W_i}{\bar{\rho}} t_0. \tag{46}$$

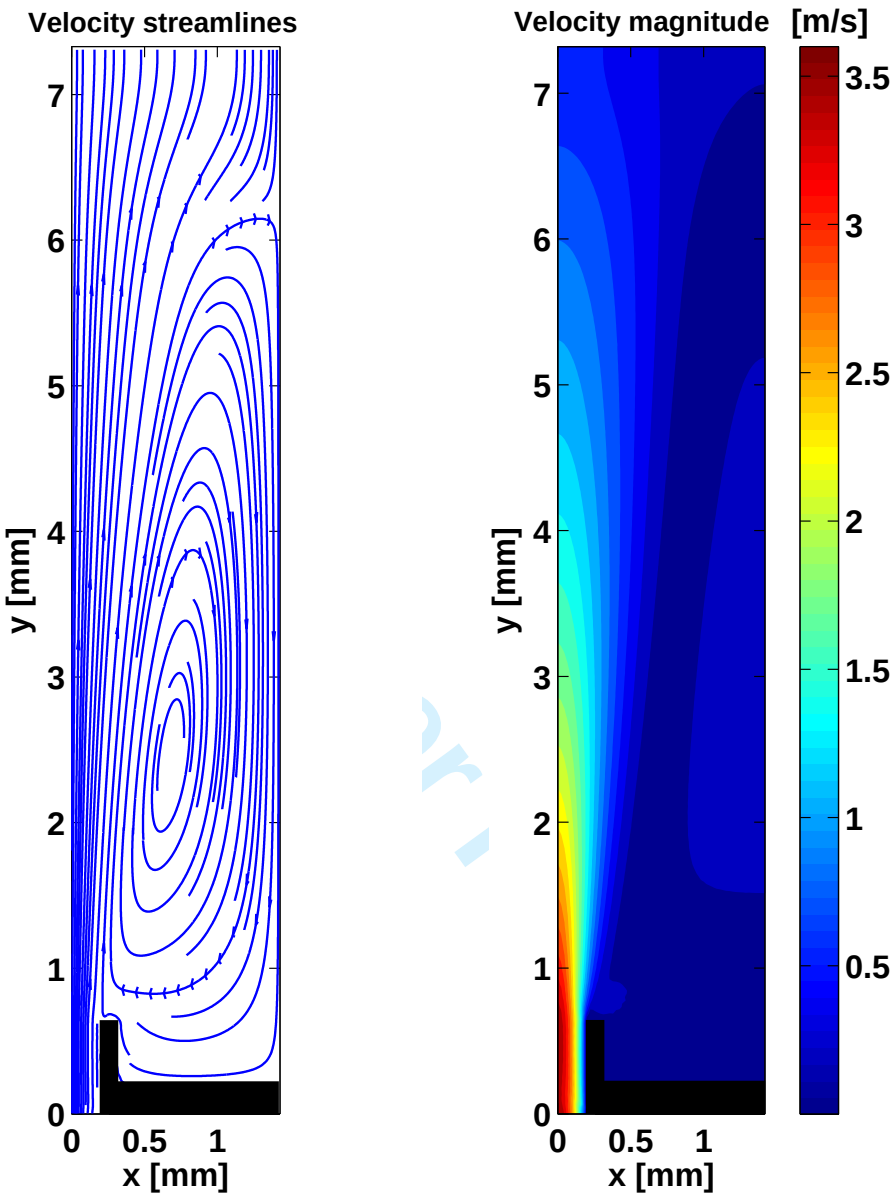

FIGURE 6. Streamlines and Euclidean norm of the velocity field in the computational domain after 120000 LB steps.

5.2. **Flow field computation.** In this simulation, we make use of a $65(Nx) \times 330(Ny)$ regular lattice, and impose constant kinematic viscosity : $\nu = 1.5 \times 10^{-5}[m^2/s]$. At the inlet, we impose the equilibrium populations corresponding to pressure $p = 1[bar]$, while the velocity is chosen according to a parabolic profile, with maximum value: $u_{max} = 3.6[m/s]$. Symmetry condition is imposed using the *mirror bounce-back* scheme to the missing populations, along the vertical boundaries of the computational domain:

$$p_x = p_{mx}, \quad p_{xy} = p_{mxy}, \quad p_{xmy} = p_{mxmy}$$
$$p_{mx} = p_x, \quad p_{mxy} = p_{xy}, \quad p_{mxmy} = p_{xmy} \tag{47}$$

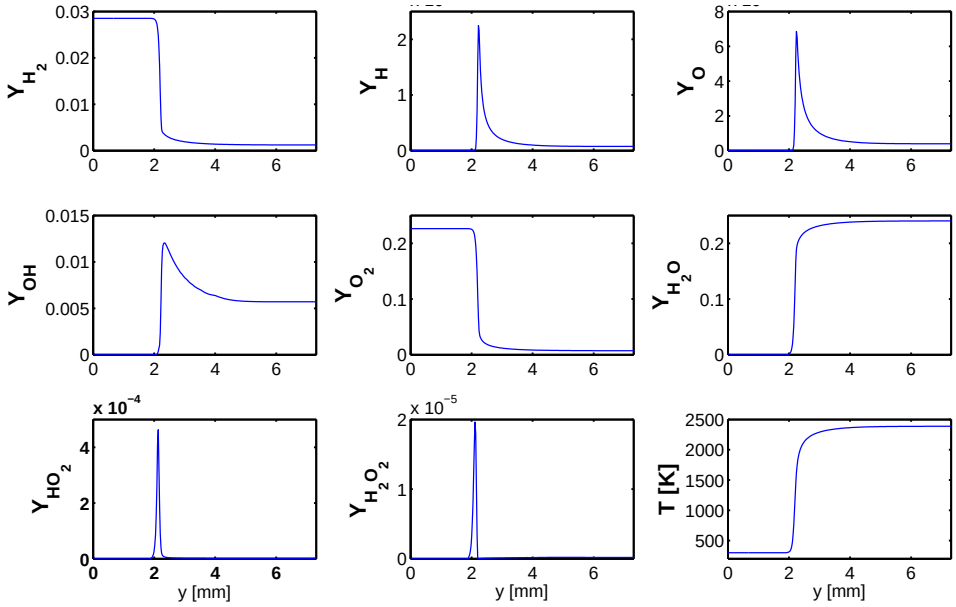

FIGURE 7. Profiles of the species mass fraction and temperature along the nozzle centerline at the time instant $t = 2.2667[ms]$.

for the left and right boundary, respectively. At the outlet, fully developed boundary condition is used by zeroth order extrapolation of the second uppermost node:

$$p_\alpha(i, N_y) = p_\alpha\left(i, N_y - 1\right), \quad i = 1, ..., N_x. \tag{48}$$

Finally, walls are treated imposing the *usual bounce back* condition: for instance, the inner wall of the nozzle is simulated as follows:

$$p_{mx} = p_x, \quad p_{mxy} = p_{xmy}, \quad p_{mxmy} = p_{xy}. \tag{49}$$

In Fig. 6, we report both the streamlines and the magnitude (Euclidean norm) of the velocity field after a large (120000) number of LB steps.

5.3. **Species computation.** Dynamics of species mass fraction and temperature field have been computed by means of the equations (42), whereas ξ^1, ξ^2 represent, according to (25), the total number of moles and the free oxygen, respectively and parameterize a two-dimensional invariant grid constructed under fixed enthalpy $\bar{h} = 2.8[kJ/kg]$ and pressure $p = 1[bar]$ at stoichiometric proportion (corresponding to the temperature $300K$ of the unburned mixture). As illustrated in section 4.3 in the case of a homogeneous batch reactor, primitive variables can be afterwards reconstructed via multi-variate interpolation using the invariant grid. Similarly to the pressure populations, the mirror-bounce back scheme (47) is adopted in order to impose symmetry condition on the vertical boundaries of the domain. Usual bounce-back condition (49) is used for simulating the adiabatic wall of the nozzle, while the equilibrium populations corresponding to the fresh mixture computed with a fixed parabolic velocity profile are maintained at the inlet. Finally, at the outlet, we make use of the following extrapolation:

$$\xi^i_\alpha\left(i, N_y\right) = \xi^i_\alpha\left(i, N_y - 1\right), \quad i = 1, \ldots, N_x. \tag{50}$$

Here, the species mass fraction and the temperature field, along the nozzle centerline, are reported in Fig. 7, whereas in Fig. 8 and 9 we report a sequence of snapshots of the time and space evolution of the O radical. It has been demonstrated [18] that the above methodology for model reduction is indeed

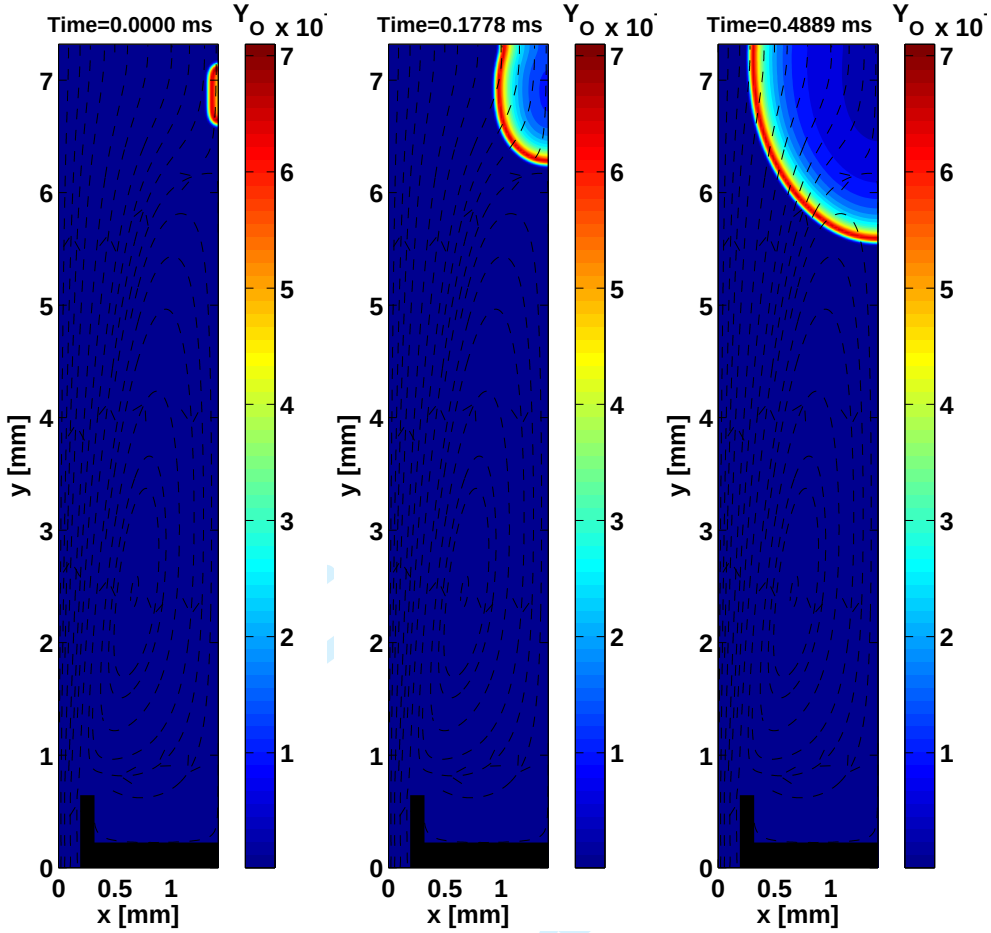

FIGURE 8. Sequence of snapshots representing the time and space evolution of O radical.

able to reproduce results of the detailed model in section 3 with great accuracy when dealing with one-dimensional flames of air and hydrogen. Nevertheless, It is worth noticing that results of the present study have been obtained at a fraction of the cost required to solve the full set of equations of section 3. Fist of all, the major drawback of lattice Boltzmann solvers for reactive flows, namely the huge number of fields to solve for and store in the memory, is addressed: in the present case only one quarter of the fields are taken into account. To this respect, the savings in terms of memory and computational time can become even more significant, as soon as we start dealing with detailed hydrocarbon mechanisms where the number of degrees of freedom are much larger (typically hundreds chemical species are involved in the reaction).

Second of all, the chemical source terms introduce stiffness in the species equations (14), hence their solution requires a sufficiently short time step δt, able to describe the fastest time scale in the problem. In particular, an estimate of time scales, due to chemistry, can be found performing an eigenvalue analysis of the Jacobian matrix $\boldsymbol{J} = [\partial f_i / \partial Y_j]$. In our case, the matrix $\boldsymbol{J}$ computed at the steady state

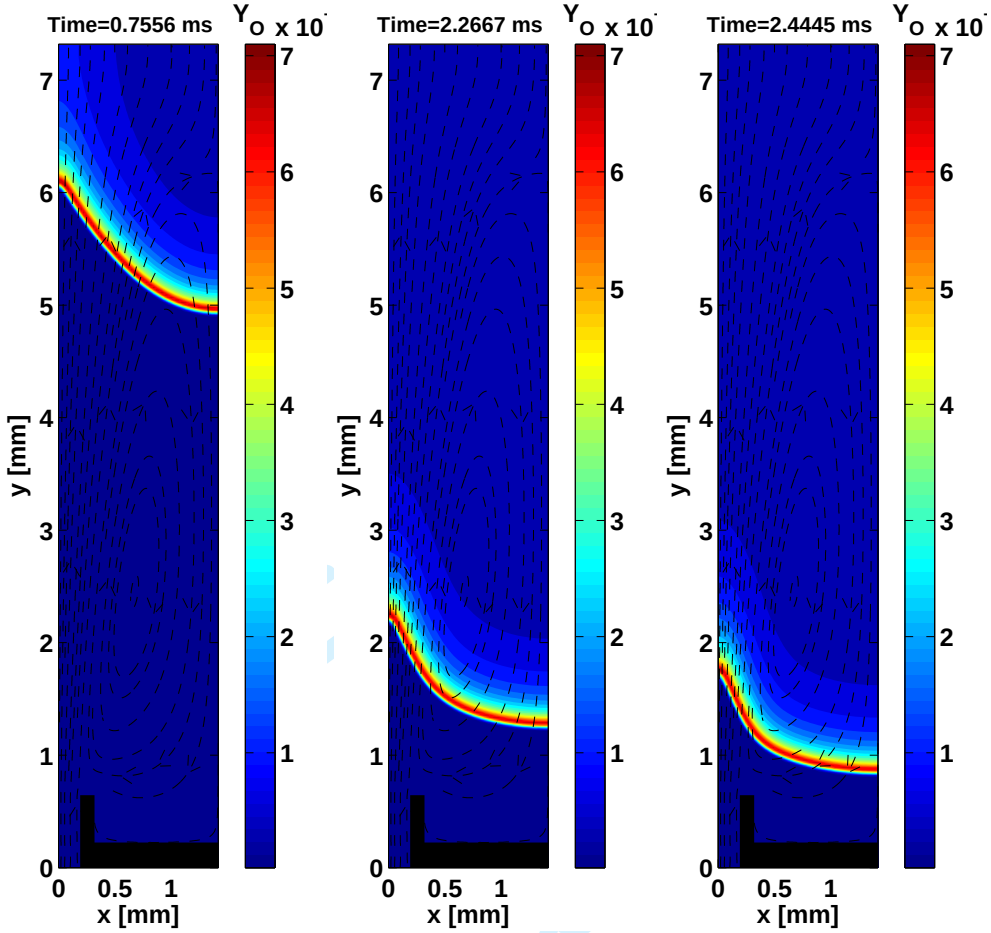

FIGURE 9. Sequence of snapshots representing the time and space evolution of O radical.

condition (fully burned mixture) exhibits the following time scales $|1/\lambda_i|$:

$$\frac{1}{|\lambda_1|} \simeq 2 \times 10^{-4}, \frac{1}{|\lambda_2|} \simeq 7.7 \times 10^{-6}, \frac{1}{|\lambda_3|} \simeq 4.4 \times 10^{-7}, \quad (51)$$
$$\frac{1}{|\lambda_4|} \simeq 2.5 \times 10^{-7}, \frac{1}{|\lambda_5|} \simeq 2.2 \times 10^{-7}, \frac{1}{|\lambda_6|} \simeq 1.5 \times 10^{-7},$$

where $|\lambda_i|$ is the absolute value of an arbitrary non-zero eigenvalue of $\boldsymbol{J}$. Hence, when solving the detailed model of section 3, the time step cannot be chosen larger than $\delta t \simeq 1 \times 10^{-7}[s]$. Notice, however, that for the simulation results of Fig. 7, 8 and 9, the technique suggested in section 5 enables us to choose a time step $\delta t = 3 \times 10^{-6}$, with an additional saving of around thirty times in terms of computational time. Finally, the present setup has been computed on a single $2GHz$ CPU double core with $4GB$ RAM memory, and it takes $2.3[s]$ in order to complete a time step: streaming, collision, rates computation and reaction sub-steps.

6. DISCUSSION AND OUTLOOK

It is worth noticing that, here the coupling of the model reduction procedure MIG and the lattice Boltzmann model in [21] has been obtained, without loss of generality, under some assumptions, which can

be gradually relaxed depending on the level of complexity that one can afford. Let's focus for now on low-Mach number combustion, where the total mixture pressure can be safely assumed constant. Above, we have considered the case of equal diffusivity and Lewis number $Le = 1$ for all the species: this guarantees that both the element mole numbers N_k in (11) and the mixture averaged enthalpy $\bar{h}$ remain constant in the domain. One more degree of freedom can be added to the problem, if we assume equal diffusivity for all the species with the Lewis number $Le \neq 1$. Now, the element composition is still conserved, while the enthalpy $\bar{h}$ varies in the domain according to the equation (19): the reduced model is fully described by the chemical coordinates ξ^i, the mixture enthalpy $\bar{h}$, and the construction, illustrated in section 4 for batch reactors, is to be performed over a range of enthalpies. In the general case, also the element composition varies, due to differential diffusion effects, and additional equations for N_k shall be solved:

$$\bar{\rho}\left(\partial_t N_k + u_j \partial_j N_k\right) = \partial_j \left(\bar{\rho} \partial_j \left(\sum_{i=1}^{n} \frac{D_i \mu_{ik} Y_i}{W_i} \right) \right), \tag{52}$$

since the reduced model is completely described by the chemical coordinates ξ^i, $\bar{h}$ and N_k. The equation (52) can be also written in the diffusion, advection and reaction form (like (13) and (14)):

$$\bar{\rho}\left(\partial_t N_k + u_j \partial_j N_k\right) = \partial_j \left(\bar{\rho} \bar{D}_k \partial_j N_k \right) + \partial_j \left(\bar{\rho} N_k \partial_j \bar{D}_k \right), \tag{53}$$

where both the diffusion coefficient

$$\bar{D}_k = \left(\sum_{i=1}^{n} \frac{D_i \mu_{ik} Y_i}{W_i} \right) \Big/ N_k \tag{54}$$

and the source term $\partial_j \left(\bar{\rho} N_k \partial_j \bar{D}_k \right)$ can be tabulated as functions of the grid parameters.

It has been found that the laminar flame speed s_L of the current setup is around $2.2[m/s]$, and it is in good agreement with experimental data [18]. Hence, we would expect that, in the case discussed in section 5, the flame assumes the typical triangular shape with the uppermost vertex located on the nozzle centerline at around $y = 2.1[mm]$, after stabilizing (see also Fig. 6 and 9). Nevertheless, we have noticed from the computations that the flame stabilization does not occur, while it continues till the inlet.

We believe that, the simple lattice Boltzmann model of Yamamoto et al. [21] is not capable to correctly predict this phenomenon, mainly due to the assumption of decoupling the flow field from the chemical reaction. Indeed, the stabilization occurs at the points of the domain where the flow becomes orthogonal to the flame with a velocity equals to s_L: however, the current model neglects both flow diffraction and acceleration through the flame front. Therefore, the present study motivates additional investigations in the near future, where the incompressible description for the flow field (12) and (15) shall be substituted with compressible models like the one suggested in [23].

7. Conclusions

Here, we suggest a promising methodology for using accurate reduced chemical kinetics in combination with a lattice Boltzmann solver in reactive flows simulations. It has been shown that the method of invariant grids (MIG) is suitable for providing the reduced description of detailed chemistry, and this approach enables to cope with stiffness introduced by chemical source terms when solving species equations. Moreover, with the help of a two dimensional laminar flame computation, we have demonstrated that, model reduction procedures are twofold beneficial because they allow to both drastically increase the time step and reduce the number of fields to solve for: The above features are particularly

desirable in the lattice Boltzmann method, where the number of fields is significantly larger than conventional methods, and explicit time scheme is adopted. Finally, possible extensions and improvements to the current study are worked out.

REFERENCES

[1] H. Rabitz, *Chem. Rev.*, vol. 87, pp. 101–112, 1987.

[2] V. I. Bykov, G. S. Yablonskii, T. A. Akramov, *Dokl. Akad. Nauk. SSSR (Doklady Chemistry)*, vol. 234(3), pp. 621–634, 1977.

[3] V. I. Dimitrov, *Reaction kinetics and catalysis Letter*, vol. 7(1), pp. 111–114, 1977.

[4] C. E. Frouzakis, K. Boulouchos, *Comb. Sci. Tech.*, vol. 159, pp. 281–303, 2000.

[5] S. H. Lam, D. A. Goussis, *Int. J. Chem. Kinet.*, vol. 26, pp. 461–486, 1994.

[6] U. Maas, S. B. Pope, *Combust. Flame*, vol. 88, pp. 239–264, 1992.

[7] Z. Ren, S. B. Pope, A. Vladimirsky, J. M. Guckenheimer, *Jour. Chem. Phys.*, vol. 124, 114111, 2006.

[8] D. Lebiedz, *Jour. Chem. Phys.*, vol. 120, 6890–6897, 2004.

[9] A. Gorban, I. V. Karlin, *Invariant Manifolds for Physical and Chemical Kinetics*. Springer, Berlin, 2005.

[10] A. N. Gorban, I. V. Karlin, A. Y. Zinovyev, *Physica A*, vol. 333, pp. 106–154, 2004.

[11] J. Li, Z. Zhao, A. Kazakov, F.L. Dryer, *Int. J. Chem. Kinet.*, vol. 36, pp. 566–575, 2004.

[12] Q. Tang, S. B. Pope, *Combust. Theory Model.*, vol. 8, pp. 255–279, 2004.

[13] H. Hamiroune, P. Bishnu, M. Metghalchi, J. C. Keck, *Combust. Theory Model.*, vol. 2, pp. 81–94, 1998.

[14] J. C. Keck, D. Gillespie, *Combust. Flame*, vol. 17, pp. 237–241, 1971.

[15] E. Chiavazzo, I. V. Karlin, *Jour. Comput. Phys.*, vol. 227, pp. 5535–5560, 2008.

[16] E. Chiavazzo, A.N. Gorban, I.V. Karlin, *Comm. Comput. Phys.*, vol. 2, pp. 964–992, 2007.

[17] E. Chiavazzo, I.V. Karlin, C.E. Frouzakis, K. Boulouchos, *Proc. Combust. Instit.*, vol. 32, pp. 519-526, 2009.

[18] E. Chiavazzo, I. V. Karlin, A. N. Gorban, K. Boulouchos, *JSTAT*, P06013, 2009.

[19] E. Chiavazzo, *Invariant Manifolds and Lattice Boltzmann method for Combustion* Ph.D. thesis, Swiss Federal Institute of Technology, ETH-Zurich, N. 18233, 2009.

[20] A. Gorban, I.V. Karlin, *Physica A*, vol. 190, pp. 393–404, 1992.

[21] K. Yamamoto, X. He, G. D. Doolen *Jour. Stat. Phys.*, vol. 107, pp. 367–383, 2002.

[22] S. Arcidiacono, I. V. Karlin, J. Mantzaras, and C. E. Frouzakis, *Phys. Rev. E*, vol. 76, 046703, 2007.

[23] N. Prasianakis and I. V. Karlin, *Phys. Rev. E*, vol. 76, 016702, 2007.

[24] P. L. Bhatnagar, E. P. Gross, M. Krook, *Phys. Rev.*, vol. 94(3), pp. 511-525, 1954.

[25] S. Succi, *The Lattice Boltzmann Equation for Fluid Dynamics and Beyond*. Oxford University Press, Oxford, 2001.

[26] I. V. Karlin, A. Ferrante, H. C. Öttinger, *Europhys. Lett.*, vol. 47(2), pp. 182–188, 1999.

[27] S. Chapman, T.G. Cowling, *The mathematical theory of non-uniform gases*. Cambridge University Press, Cambridge, 1970.

[28] S. Chen, G. Doolen, *Annu. Rev. Fluid Mech.*, vol. 30, pp. 329–364, 1998.

Title: Efficient simulations of detailed combustion fields via the lattice Boltzmann method

Journal: International Journal of Numerical Methods for Heat and Fluid Flow

Author(s):

1) Eliodoro Chiavazzo (eliodoro.chiavazzo@polito.it)
Politecnico di Torino, Corso Duca degli Abruzzi 24, 10129 Torino Italy.

2) Ilya V. Karlin (karlin@lav.mavt.ethz.ch)
Swiss Federal Institute of Technology (ETH), Institut f. Energietechnik ML L 13 Sonneggstrasse 3 8092 Zurich Switzerland.

3) Alexander N. Gorban (ag153@leicester.ac.uk)
University of Leicester, Department of Mathematics University road LE1 7RH Leicester UK.

4) Konstantinos Boulouchos (boulouchos@lav.mavt.ethz.ch)
Swiss Federal Institute of Technology (ETH), Institut f. Energietechnik ML J 39 Sonneggstrasse 3 8092 Zurich Switzerland.